Springer

KSME

Journal of Mechanical Science and Technology 25 (6) (2011) 1475~1482
www.springerlink.com/content/1738-494x
DOI 10.1007/s12206-011-0405-0

Diagnostic flow metering using ultrasound tomography †

Sejong Chun[1,*], Byung-Ro Yoon[1] and Kwang-Bock Lee[2]

[1]*Division of Physical Metrology, Korea Research Institute of Standards and Science, Daejeon, 305-340, Korea*
[2]*Hitrol Co. Ltd., Paju-si, Gyeonggi-do, 413-824, Korea*

(Manuscript Received July 6, 2010; Revised March 4, 2011; Accepted March 9, 2011)

Abstract

For an accurate flow metering without considering the influences of flow control devices such as valves and elbows in closed conduits, velocity distribution in the cross-sectional area must be integrated. However, most flow meters, including multi-path ultrasonic, electromagnetic or Coriolis mass flow meters, require assumptions on the fully-developed turbulent flows to calculate flow rates from physical quantities of their own concern. Therefore, a long straight pipe has been a necessary element for accurate flow metering because the straight pipe can reduce flow disturbances caused by flow control devices. To reduce costs due to the installation of long straight pipes, another flow metering technique is required. For example, flow rates can be estimated by integrating velocity distributions in the cross-section of conduits. In the present study, ultrasound tomography was used to find the velocity distribution in the cross-section of a closed conduit where flow was disturbed by a Coriolis mass flow meter or a butterfly valve. A commercial multi-path ultrasonic flow meter was installed in the pipeline to measure the line-averaged velocity distribution in the pipe flow. The ultrasonic flow meter was rotated 180° at intervals of 10° to construct line-averaged velocity distributions in Radon space. Flow images were reconstructed by using a back-projection algorithm (inverse Radon transform). Flow diagnostic parameters were defined by calculating statistical moments, i.e., average, standard deviation, skewness, and kurtosis, based on the normalized velocity distribution. The flow diagnostic parameters were applied to flow images to find whether the parameters could discern flow disturbances in the reconstructed velocity distribution.

Keywords: Computed tomography; Flow metering; Radon transform; Ultrasonic flow meter

1. Introduction

For accurate flow metering in water or crude oil pipelines, velocity distributions in the pipelines should have characteristics of fully-developed turbulent flow. Straight pipelines are installed upstream of flow meters to ensure fully-developed turbulent flows. The length of straight pipes must be long enough to reduce flow disturbances by valves or elbows in moderate Reynolds numbers [1]. However, unexpected flow disturbances, such as an abrupt increase in upstream pressure, can influence flow conditions to make flow metering incorrect. To evaluate such effects of flow disturbances on flow metering, velocity distributions in the pipe flows must be found.

Ultrasound tomography is a means of reconstructing flow images from line-averaged velocity distribution by inverse Radon transform [2-7]. In the literature, ultrasound tomography has been implemented by using 16 ultrasonic transducers for flow image reconstruction purposes [3, 4]. Eight ultrasonic transducers were installed on the upstream side, and the other eight ultrasonic transducers were installed on the downstream side of the flow metering section. Such arrangement of ultrasonic sensors created 64 ultrasonic paths for reconstructing flow images. Therefore, an ultrasonic flow meter had to be specially made for flow image reconstruction purposes.

In the case of using a commercial multi-path ultrasonic flow meter, the flow meter must be rotated with respect to the pipe axis for ultrasound tomography. This can be implemented by installing two rotational pipe rigs at both sides of the flow meter. By rotation of the ultrasonic flow meter at small angular intervals, the line-averaged velocity distribution can be mapped into Radon space. The back-projection algorithm (inverse Radon transform) is then performed to reconstruct a flow image from the line-averaged velocity distribution [2-4].

Flow diagnostic parameters are derived from mean flow velocity distribution to verify the flow conditions as to whether the velocity profile is fully-developed turbulent or not [8-11]. While most of the previous works have focused on the self-validation of flow metering in a metering station in applications with wireless sensor networks, some other works have suggested flow diagnostic parameters to investigate flow conditions by examining the mean flow velocity profile. Hydrodynamic factors, which are a ratio between the theoretical and

† This paper was recommended for publication in revised form by Associate Editor Simon Song

*Corresponding author. Tel.: +82 42 868 5311, Fax.: +82 42 868 5028
E-mail address: sjchun@kriss.re.kr

the measured mean flow velocity, or orientation sensitivity factors, which are derived from the difference of the hydrodynamic factors, were suggested to emphasize the efficacy of tomographic flow metering compared with the conventional flow metering (diametrical or multi-path transit-time ultrasonic methods) [3]. However, there were no flow diagnostic parameters to look at the shapes of the mean flow velocity profiles with respect to statistical moments.

Statistical moments can provide better estimates of flow diagnosis because the statistical moments can give some information regarding the flow conditions of the pipe flows if the mean flow velocity distribution is normalized as a function similar to a probability density function. Four statistical moments such as average, standard deviation, skewness, and kurtosis can be considered as candidates as flow diagnostic parameters. The notions of the statistical moments are different from the definition of statistical moments in turbulent flows because the present definition stems from the spatial distribution of mean flow velocity profiles. If the statistical moments are good enough to discern different flow disturbances in the pipe flows, the statistical moments can provide indicators for diagnosing flow conditions for accurate flow metering.

In the present study, a commercial multi-path transit-time ultrasonic flow meter was used to reconstruct flow images based on line-averaged velocity distribution [12, 13]. Toward this end, two rotational rigs were attached on both sides of the ultrasonic flow meter to give angular intervals during flow metering. A Coriolis mass flow meter and a butterfly valve were used to create flow disturbances. Statistical moments were calculated to find whether they can be used as flow diagnostic parameters. The statistical moments were also calculated with the theoretical flow velocity profiles, in which the fully-developed laminar and turbulent flows were assumed, to compare them with the measured statistical moments. It was found that skewness and kurtosis were appropriate as flow diagnostic parameters in the flows downstream of the Coriolis flow meter and the butterfly valve.

2. Experimental apparatus and experimental methods

The water flow rate facility in KRISS was used to implement ultrasound tomography using a commercial multi-path ultrasonic flow meter (UR-1000 Plus, CMNTech, Inc.). The expanded uncertainty (k = 2.01 with a confidence level of 95%) of the water flow rate facility was less than 0.072%. The flow rate in the facility was changed by controlling three glove valves downstream of a test section in the range between 50 m^3/h and 200 m^3/h. During flow measurements, pressure upstream of the test section was maintained at 190 kPa due to the constant head tank in the flow rate facility. The temperature in the pipeline was measured to be between 31°C and 33°C.

Fig. 1(a) shows schematic diagrams for the experimental setup downstream of a mass flow meter (PROMASS83, Endress+Hauser, Inc.) and a butterfly valve (F001, Keystone Valve Corp.). The length of straight pipe downstream of the mass flow meter was short at less than 2D, where D was the pipe diameter of 100 mm. The non-dimensional distance between the outlet of the mass flow meter and the center of ultrasonic flow meter was 5.5D. An electromagnetic flow meter (PROMAG 53, Endress+Hauser, Inc.) was installed downstream of the ultrasonic flow meter to monitor the flow rates in the pipe flow. When the butterfly valve was installed, the length of the straight pipe was either 5.5D or 14.5D, as shown in Fig. 1(b). The closing angle of the butterfly valve, ϕ was defined as 0°, 30°, 45°, and 60° to define various levels of flow disturbance to the test section. Flow disturbances were expected to increase when ϕ was increased. Swirling flows were also expected by increasing the valve closing angle.

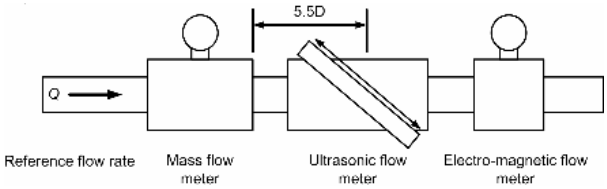

(a) Liquid flow after a mass flow meter

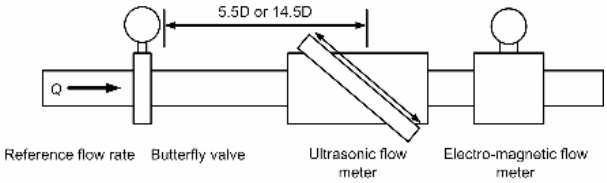

(b) Liquid flow after a butterfly valve

Fig. 1. Experimental setup for ultrasound tomography.

Two rotational rigs were attached on the upstream and downstream sides of the ultrasonic flow meter to implement ultrasound tomography. The rotational rigs enabled the flow meter to be rotated at angular intervals of 10° around the pipe axis. The rotational angle was measured by using an angle level meter (AL-12, Iwatsu, Inc.) with a resolution of ±0.5°. The ultrasonic flow meter used for five ultrasonic paths to measure flow rates. By considering no-slip conditions at the pipe wall, two additional dummy paths with zero line-averaged velocities were attached to the five ultrasonic paths to better describe the mean flow velocity distribution in the pipe. Therefore, 133 data (7 ultrasonic paths × 19 angles between 0° and 180°) were obtained to reconstruct the flow profiles. The measurement volume by ultrasound tomography was 246.7 cm^2 × 7.1 cm = 1751.6 cm^3.

At each measurement point, 20 samples were measured at intervals of 1 s. Because the flow regime in the pipe flow was turbulent with Reynolds numbers in the range from Re = 170,000 to 700,000, both the sampling rate and the number of samples should have been large enough to describe turbulent flows. However, this was not possible because of the limitations of the sampling rate in the commercial ultrasonic flow meter. To overcome such problems, a high scan-rate pulser &

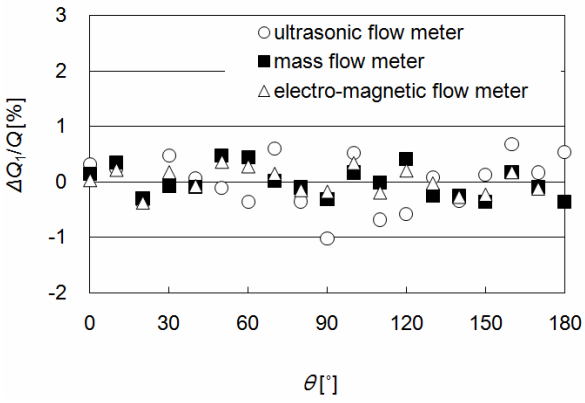

(a) $\Delta Q_1/Q$

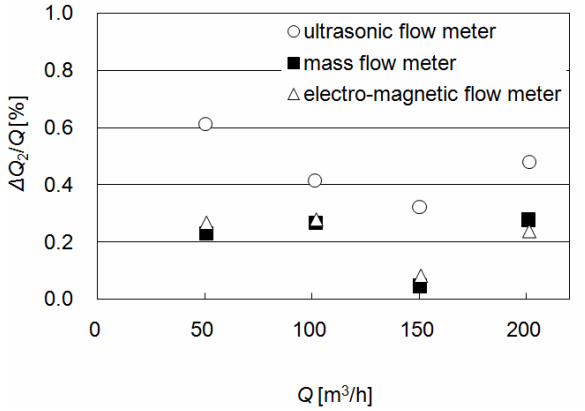

(b) $\Delta Q_2/Q$

Fig. 2. Variation of flow rates in flow measurements downstream of a mass flow meter.

Table 1. Spatial resolution of ultrasound tomography.

Radon space	inverse Radon space	spatial resolution
7 × 18	4 × 4	25 mm × 25 mm
50 × 181	34 × 34	2.9 mm × 2.9 mm
100 × 181	70 × 70	1.4 mm × 1.4 mm
200 × 181	170 × 170	0.6 mm × 0.6 mm

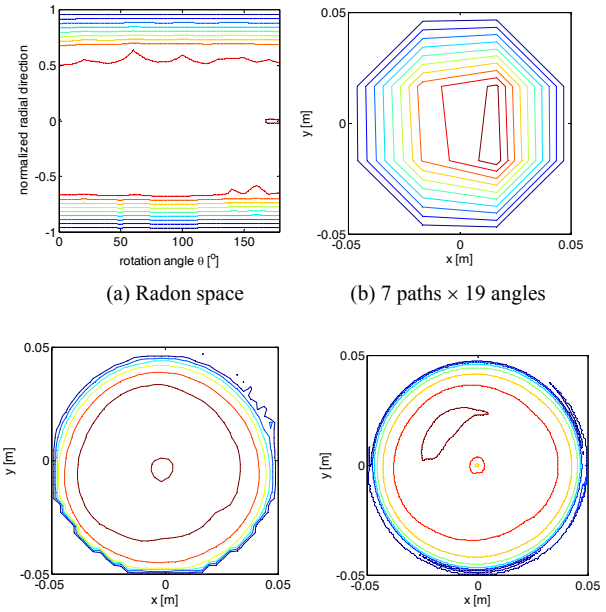

(a) Radon space (b) 7 paths × 19 angles

(c) 50 paths × 181 angles (d) 200 paths × 181 angles

Fig. 3. Reconstruction of flow image by an inverse Radon transform (Q = 150 m^3/h, z/D = 5.5).

receiver board can be considered to replace the commercial flow meter [14]. However, the main purpose of this study was focused on the reconstruction of the mean flow velocity distribution by using the back-projection algorithm. In this regard, the low sampling rate and small number of data might be acceptable in measuring the mean flow velocity distribution in a well-defined flow condition, i.e., the fully-developed turbulent flow. In strong swirling flows, it was expected that the accuracy of reconstructing flow images would be deteriorated by the above-mentioned insufficient sampling rate and the sample numbers.

Fig. 2(a) shows relative deviations of flow rate with respect to rotational angle θ at Q = 200 m^3/h, where Q is the reference flow rate upstream of the mass flow meter or the butterfly valve, as shown in Fig. 1. ΔQ_1 denotes the deviations of Q measured at a specified θ from the averaged value of Q. $\Delta Q_1/Q$ shows relative deviations less than ±1% during the flow measurement with rotation of the ultrasonic flow meter at Q = 200 m^3/h. To summarize $\Delta Q_1/Q$ at various flow rates, the relative standard deviation of Q, namely, $\Delta Q_2/Q$, is introduced in Fig. 2(b). $\Delta Q_2/Q$ indicates the relative standard deviations of less than 0.6% in the case of the ultrasonic flow meter and 0.4% in the case when both the mass flow meter and the electro-magnetic flow meter are in the range of Q = 50 ~ 200 m^3/h.

An example of a reconstructed flow image is shown in Fig. 3, when the flow is measured downstream of the mass flow meter at Q = 150 m^3/h. The measured data are displayed in Radon space. The data are transformed into real space by an inverse Radon transform. When the measured data (7 paths × 19angles) are transformed without interpolation in Radon space, the reconstructed flow image suffers from insufficient resolution, as indicated in Fig. 3(b) [3, 4]. The spatial resolution of reconstructed flow image becomes 25 mm, as shown in Table 1. By interpolating the measured data with a finer mesh, the reconstructed image becomes better, as shown in Figs. 3(c) and 3(d). With the finest interpolation in Radon space (200 paths × 181 angles), the spatial resolution becomes 0.6 mm. This is a necessary procedure because both the number of ultrasonic paths and the angular resolution are constrained in the present experimental setup. After interpolating the measured data in Radon space, the back projection algorithm is applied to reconstruct the flow image by inverse Radon transform [2-4]. In this study, the iradon function of the image processing toolbox in MATLAB (Mathworks Inc.) was used to implement the back projection algorithm [15].

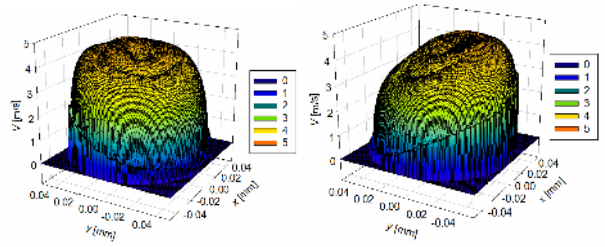

(a) angle 0° (b) angle 30°

Fig. 4. Reconstruction of flow images downstream of a butterfly valve (Q = 100 m^3/h, z/D = 5.5).

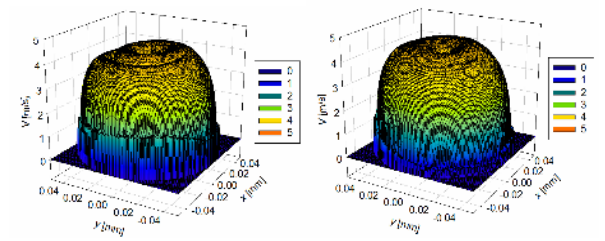

(a) angle 0° (b) angle 30°

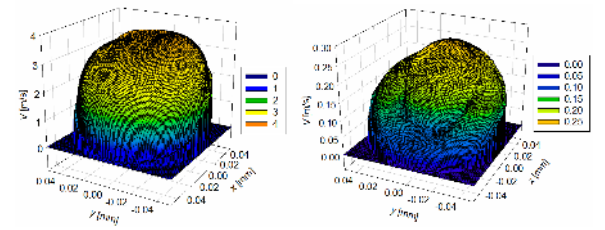

(c) angle 45° (d) angle 60°

Fig. 5. Reconstruction of flow images downstream of a butterfly valve (Q = 100 m^3/h, z/D = 14.5).

3. Experimental results and discussion

Fig. 4 shows reconstructed flow images downstream of the butterfly valve when Q = 100 m^3/h and z/D = 5.5 with the valve closing angle ϕ between 0° and 30°. Some ultrasonic paths showed error signals when ϕ was increased to greater than 45° due to strong swirling flows. The reconstructed flow images show annular stripes due to the limitations of the commercial ultrasonic flow meter and the annular stripes are not removed by increasing mesh sizes for interpolating the measured data. The shape of the mean flow velocity profile at ϕ = 0° seems to be symmetrical, while the profile shape at ϕ = 30° becomes skewed, as seen in Fig. 4(b).

The reconstructed flow images are influenced by increasing the valve closing angle ϕ at z/D = 14.5, as shown in Fig. 5. At first, the magnitudes of the reconstructed flow images are decreased by increasing ϕ. At the same time, the skewness of the flow images can be seen as increasing ϕ. The blunt shape of flow images also changes into sharper images with increasing ϕ. This is due to the swirling flows behind the butterfly valve, which is partially-closed.

Based on the observations of the reconstructed flow images, the flow diagnostic parameters can be derived by defining statistical moments of the normalized velocity profiles $U(x, y)$ as follows:

$$(x_1, y_1) = \left(\int xU(x,y)dx, \int yU(x,y)dy \right) \tag{1}$$

$$(x_2, y_2) = \left(\left(\int (x-x_1)^2 U(x,y)dx \right)^{0.5}, \left(\int (y-y_1)^2 U(x,y)dy \right)^{0.5} \right) \tag{2}$$

$$(x_3, y_3) = \left(\frac{\int (x-x_1)^3 U(x,y)dx}{x_2^3}, \frac{\int (y-y_1)^3 U(x,y)dy}{y_2^3} \right) \tag{3}$$

$$(x_4, y_4) = \left(\frac{\int (x-x_1)^4 U(x,y)dx}{x_2^4}, \frac{\int (y-y_1)^4 U(x,y)dy}{y_2^4} \right). \tag{4}$$

Here, $U(x, y)$ is the normalized velocity profile without physical units, and it satisfies the following equation:

$$\int\int U(x,y)dxdy = 1 \tag{5}$$

(x_1, y_1), (x_2, y_2), (x_3, y_3), (x_4, y_4) are denoted as the average and standard deviation, skewness and kurtosis, respectively. Therefore, $U(x, y)$ is considered as a sort of probability density function by Eqs. (1)-(5). Note that the physical dimensions of the average and the standard deviation are denoted in meters, while the skewness and the kurtosis are normalized without physical units. To construct flow diagnostic parameters, the vector sum of x_i and y_i is defined as follows:

$$z_i = \sqrt{x_i^2 + y_i^2}, \quad i = 1,2,3,4. \tag{6}$$

Here, z_i is defined as the flow diagnostic parameters.

Fully-developed laminar and turbulent flow parameters can be used as limiting values to two flow diagnostic parameters, z_2 and z_4. The normalized mean flow velocity profile in the case of the fully-developed laminar flow is defined as follows:

$$U(x,y) = \frac{2}{\pi}\left(1 - r^2\right), \quad 0 \le r \le 1. \tag{7}$$

Here, $2/\pi$ is multiplied to satisfy Eq. (5). The normalized mean flow velocity profile in the case of the fully-developed turbulent flow is denoted as follows:

$$U(x,y) = \frac{60}{49\pi}\left(1 - r\right)^{1/7}, \quad 0 \le r \le 1. \tag{8}$$

Here, $60/49\pi$ is also introduced to satisfy Eq. (5). The limiting values of flow diagnostic parameters can be calculated using Eqs. (1)-(8).

In the flows downstream of the mass flow meter, the bluntness of mean flow velocity profile in Fig. 3 can be described by using the flow diagnostic parameters z_2 and z_4 as shown in

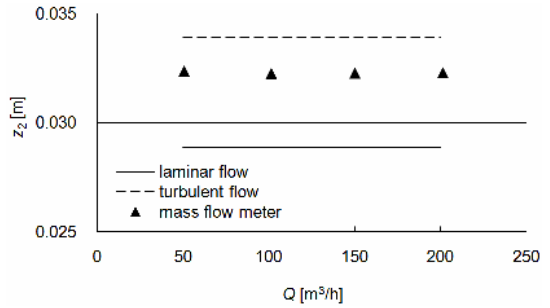

(a) z_2

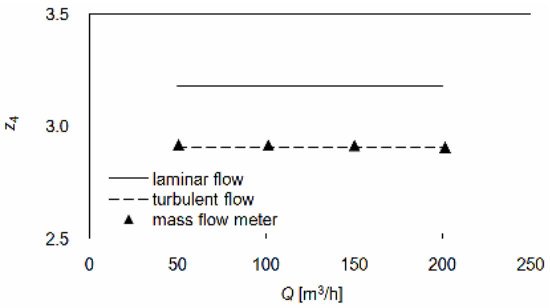

(b) z_4

Fig. 6. Flow diagnostic parameters for pipe flows downstream of the mass flow meter (z/D = 5.5).

Fig. 6. The flow diagnostic parameters show values of z_2 = 32 mm and z_4 = 2.92 by ultrasound tomography. Note that z_2 = 29 mm and z_4 = 3.18 from Eq. (7), while z_2 = 34 mm and z_4 = 2.91 from Eq. (8). Because z_2 has a value between 29 mm and 34 mm, the flow image seems to show flow characteristics of developing flow between the fully-developed laminar and turbulent flows, whereas z_4 indicates the closeness to the value of 2.91, which means that the mean flow velocity profile belongs to the fully-developed turbulent regime. Considering the Reynolds numbers in the present experiment (Re = 170,000 ~ 700,000), the reconstructed flow images belong to the turbulent flows. Because z_4 describes the bluntness of the shape of the mean flow velocity profile, z_4 can indicate the type of diagnosed flow profile downstream of the mass flow meter.

Flow diagnostic parameters in the flow at x/D = 14.5 downstream of the butterfly valve are displayed in Fig. 7. z_1 indicates the central positions of the reconstructed flow images, which increases as ϕ is increased from 0° to 60°. This is due to flow asymmetry by swirling flows downstream of the butterfly valve. z_2 indicates the standard deviations of the normalized velocity distribution, increasing from 32 mm to 34 mm when ϕ increases from 30° to 60°. There are large deviations of z_2 at ϕ = 60° due to the strong swirling flows. z_3 shows the skewness of the normalized velocity distribution. z_3 is less than 0.1 at $\phi \leq 45°$, while z_3 increases to greater than 0.2 at $\phi \geq 60°$, which indicates flow asymmetry by swirling flows downstream of the butterfly valve. Even though both z_1 and z_3 can indicate the flow asymmetry of the measured flow profile, z_3 seems to be better because z_3 is a normalized value within [-1, 1]. z_4 indicates the kurtosis of the normalized velocity distribution, which measures the bluntness of the normalized velocity distribution. At ϕ = 0°, z_4 is 2.91, which indicates fully-developed turbulent flow. z_4 is maintained at less than 2.95 at $\phi \leq 45°$, while z_4 indicates values of greater than 3 at ϕ = 60°, which means that the normalized velocity distribution at ϕ =

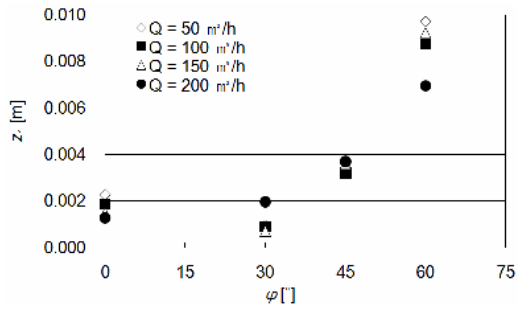

(a) z_1

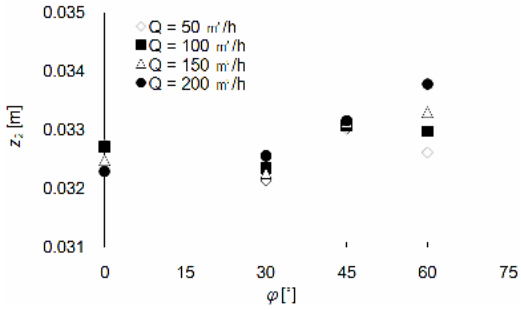

(b) z_2

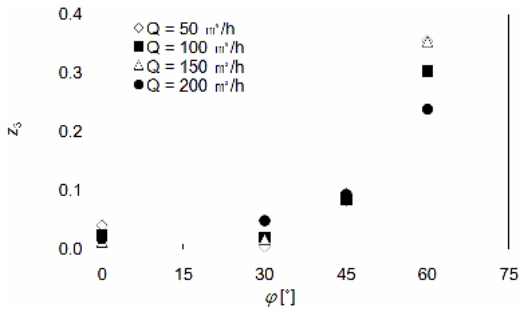

(c) z_3

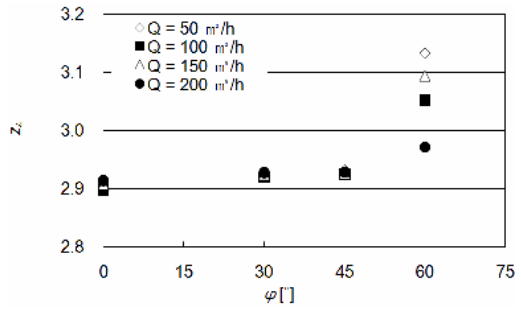

(d) z_4

Fig. 7. Flow diagnostic parameters for liquid flow downstream of the butterfly valve (z/D = 14.5).

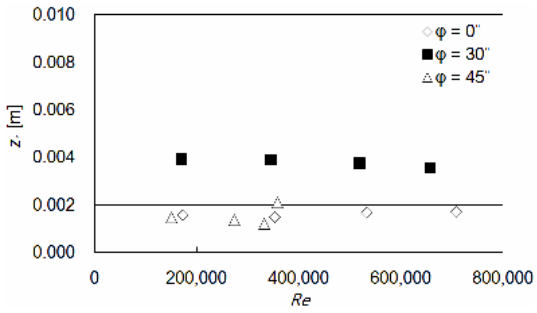

(a) z_1

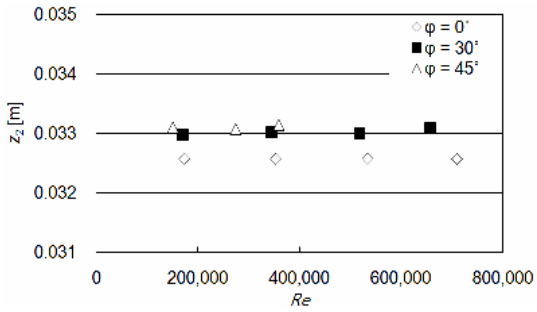

(b) z_2

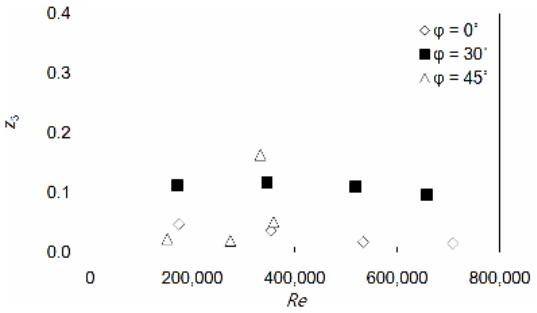

(c) z_3

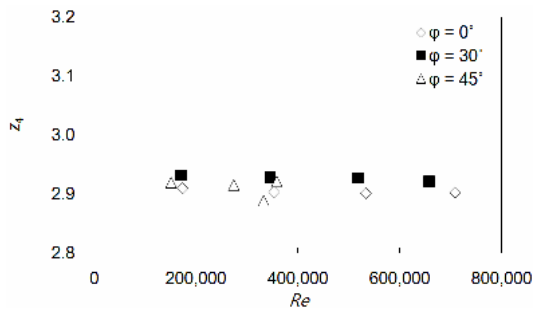

(d) z_4

Fig. 8. Flow diagnostic parameters for liquid flow downstream of the butterfly valve (z/D = 5.5).

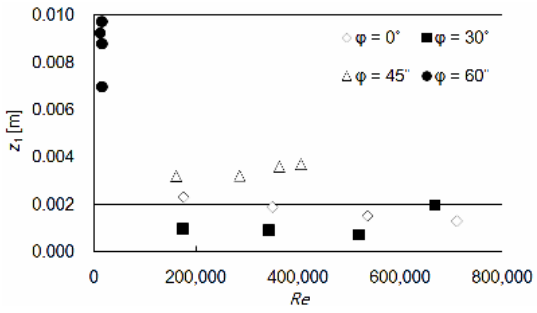

(a) z_1

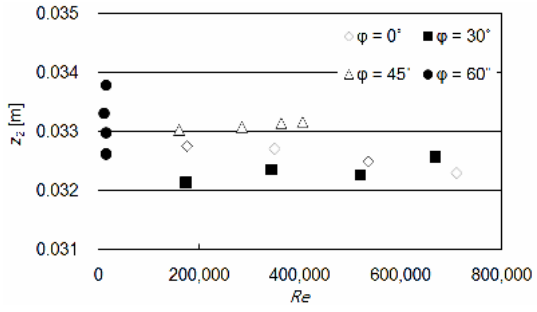

(b) z_2

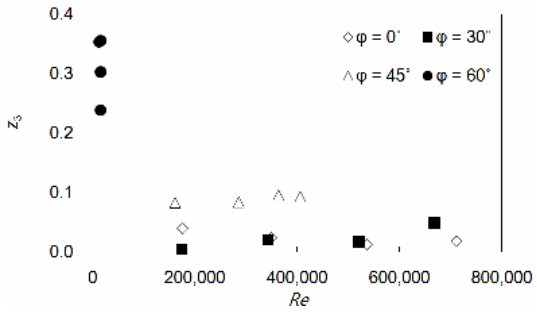

(c) z_3

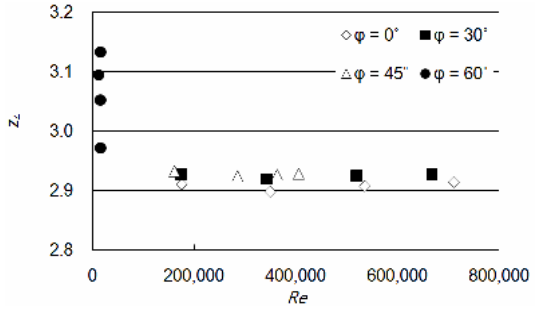

(d) z_4

Fig. 9. Flow diagnostic parameters for liquid flow downstream of the butterfly valve (z/D = 14.5).

60° shows flow characteristics of a developing flow.

The same flow diagnostic parameters are displayed with respect to the Reynolds numbers at both z/D = 5.5 and 14.5 in Figs. 8 and 9. At z/D = 5.5 and $\phi \leq 45°$, z_1 is less than 4 mm in Fig. 8(a), which indicates symmetry in the reconstructed flow images, by considering the pipe diameter of 100 mm. This tendency is observed at z/D = 14.5 and $\phi \leq 45°$ in Fig. 9(a). When z/D = 14.5 and ϕ = 60°, z_1 becomes within 6 ~ 10 mm, which indicates asymmetry of the reconstructed flow image. z_2 shows a value of around 33 mm at z/D = 5.5, a value that is similar to the reconstructed flow images downstream of the mass flow meter (Fig. 6(a)). At z/D = 14.5, z_2 is slightly de-

creased from 33 mm to 32 mm at $\phi = 0°$ and 30°. This means that the reconstructed flow images become sharper. At $\phi = 60°$, z_2 is distributed between 32.5 mm and 34 mm because the flows become unstable by presence of swirling flows. Note that the Reynolds number at $\phi = 60°$ is distributed between 11,700 and 15,500 in the present experiment.

z_3 shows the reduction of skewness in the reconstructed flow images as the flow goes downstream in Figs. 8(c) and 9(c). At $\ell/D = 5.5$ and $\phi = 30°$, z_3 is located at around 0.1, while z_3 becomes close to zero at $\ell/D = 14.5$. This means that the flow becomes symmetrical further downstream because the strength of swirling flows is weakened at this location. This tendency is consistent with z_1 in that both values are decreased as the flow goes downstream. Meanwhile, z_4 maintains values of around 2.91 in the case of $0° \le \phi \le 45°$ at both $\ell/D = 5.5$ and 14.5, shown in Figs. 8(d) and 9(d). This means that the shape of reconstructed flow images has similarity with that of the fully-developed turbulent flows ($z_4 = 2.91$). However, the value at $\phi = 60°$ is distributed between 2.95 and 3.13. This is because the flow at $\phi = 60°$ shows some characteristics of a developing flow from a laminar to a turbulent flow regime. From this discussion, it is seen that the fully-developed turbulent flow upstream of the butterfly valve is disturbed by the swirling flows at $\ell/D = 5.5$ and that the effect of swirling flow is decreased gradually to recover developing turbulent flows from the disturbed flows at $\ell/D = 14.5$.

This point can be observed by investigating z_1 and z_3 because these parameters can indicate the symmetry of the reconstructed flow images. Also, z_2 and z_4 can give information regarding the bluntness of the shape of the reconstructed flow images. When the swirling flow downstream of the butterfly valve is so strong at $\phi = 60°$, all the flow diagnostic parameters show large distribution, which indicates that flow metering at this ϕ would not be reliable because the flow is a developing flow. In particular, z_3 and z_4 give a better indication of flow diagnosis than z_1 and z_2 because they are normalized to compare themselves with limiting values, i.e., the values by assuming the fully-developed laminar and turbulent flows. Therefore, it is concluded that z_3 and z_4 would be more appropriate than z_1 and z_2 to be used as suitable flow diagnostic parameters.

These flow diagnostic parameters can be calculated whenever the mean flow velocity profiles are reconstructed by ultrasound tomography. If the mean flow velocity profiles can be reconstructed with a high sampling rate, the flow diagnostic parameters can indicate the flow conditions with real-time. This can lead to on-line monitoring in the measuring stations via a wireless sensor network, as suggested in the literature [9-11]. However, the present experiment relies on the manual rotation of an ultrasonic flow meter, which hinders the fast reconstruction of flow images. This might be resolved by introducing an automated rotational rig in combination with a high scan-rate ultrasonic flow meter. If such improvements could be done, the flow diagnostic parameters can give a means of real-time flow diagnosis for an accurate flow metering.

4. Conclusions

Flow images downstream of a mass flow meter and a butterfly valve have been reconstructed by ultrasound tomography. The back projection algorithm was used to reconstruct the flow images from the line-averaged velocity distribution in Radon space. The velocity distribution was measured by a commercial multi-path ultrasonic flow meter with two rotational rigs. Flow diagnostic parameters were suggested by defining statistical moments, namely, average, standard deviation, skewness, and kurtosis, based on the normalized mean flow velocity distributions. The normalized velocity distributions were taken as a probability density function in this study. The flow diagnostic parameters were different from the hydrodynamic factor and the orientation sensitivity factor from the previous studies in that the flow diagnostic parameters can be directly calculated from the reconstructed flow image to check symmetry and bluntness of the flow image. From the data analysis, it was found that the skewness and the kurtosis can be useful flow diagnostic parameters to describe flow disturbances by flow controlling elements such as the butterfly valve.

Acknowledgement

This work was supported by Korea Institute of Energy Technology Evaluation and Planning (KETEP) grant funded by the Ministry of Knowledge Economy in Korea (No. 2010T100100 356).

Nomenclature

D : Diameter of conduit [mm]
Q : Flow rate [m^3/h]
Re : Reynolds number
U : Normalized velocity profile [m/s]
V : Mean flow velocity in a conduit [m/s]
r : Radial direction [mm]
x_i : i-th statistical moment in x direction
y_i : i-th statistical moment in y direction
z_i : i-th flow diagnostic parameter
z : Streamwise direction [mm]
ΔQ_1 : Deviations of Q from the average of Q value at θ [m^3/h]
ΔQ_2 : Standard deviations of Q [m^3/h]
θ : Rotational angle [^{o}]
ϕ : Valve closing angle [^{o}]
ν : Kinematic viscosity [m^2/s]

References

[1] W. Merzkirch, Fluid mechanics of flow metering, *Springer,* Heidelberg, Germany (2005).
[2] T. M. Buzug, Computed tomography: from photon statistics to modern cone-beam CT, *Springer*, Heidelberg, Germany (2008).

[3] D. Kurniadi and A. Trisnobudi, A multi-path ultrasonic transit time flow meter using a tomography method for gas flow velocity profile measurement, *Part. Syst. Charact.*, 23 (2006) 330-338.
[4] R. A. Rahim, M. H. F. Rahiman, K. S. Chan and S. W. Nawawi, Non-invasive imaging of liquid/gas flow using ultrasonic transmission-mode tomography, *Sensors and Actuators A*, 135 (2007) 337-345.
[5] Warsito, M. Ohkawa, N. Kawata and S. Uchida, Cross-sectional distributions of gas and solid holdups in slurry bubble column investigated by ultrasonic computed tomography, *Chemical Engineering Science*, 54 (1999) 4711-4728.
[6] L. J. Xu and L. A. Xu, Gas/liquid two-phase flow regime identification by ultrasonic tomography, *Flow Measurement and Instrumentation*, 8 (3/4) (1997) 145-155.
[7] L. Xu, Y. Han, L. A. Xu and J. Yang, Application of ultrasonic tomography to monitoring gas/liquid flow, *Chemical Engineering Science*, 52 (13) (1997) 2171-2183.
[8] M. P. Henry, D. W. Clarke, N. Archer, J. Bowles, M. J. Leahy, R. P. Liu, J. Vignos and F. B. Zhou, A self-validating digital Coriolis mass-flow meter: an overview, *Control Engineering Practice*, 8 (2000) 487-506.
[9] M. Henry, On-line compensation in a digital Coriolis Mass Flow meter, *Flow Measurement and Instrumentation*, 12 (2001) 147-161.
[10] A. Abou-Arkoub, R. Thorn, A. Bousbaine, Online validation of multiphase flowmeters using simple capacitance sensors, *IEEE Transactions on Instrumentation and Measurement*, 59 (2010) 2671-2682.
[11] M. A. Collett, M. G. Cox, M. Duta, T. J. Esward, P. M. Harris and M. P. Henry, The application of self-validation to wireless sensor networks, *Measurement Science and Technology*, 19 (2008) 125201.
[12] S. Chun, B. –R. Yoon, K. –B. Lee and J. –S. Paik, Diagnostic flow metering using ultrasound tomography, *AIP Conference Proceedings*, 1225 (2010) 533-539.
[13] S. Chun, B. –R. Yoon and K. –B. Lee, Diagnostic flow metering using ultrasound tomography, *ISFV-14 Conference*, ISFV14-1A-5, (June 20-24, 2010) EXCO, Daegu, Korea.
[14] L. Zhang, X. Xu, C. Hu, L. Sun, J. T. Yen, J. M. Cannata and K. K. Shung, Improved high-frequency high frame rate duplex ultrasound linear array imaging system, *IEEE International Ultrasonics Symposium*, CFP08ULT-PRT 76999 (November 2-5, 2008), Beijing, China.
[15] The MathWorks, *Image processing toolbox™ 6: User's Guide*, March, Natick, MA, USA (2009) Ch.9, 30-36.

Sejong Chun is a research engineer working at KRISS in Korea. He has joined the Division of Physical Metrology since 2004. He majored in fluid mechanics for his Ph.D. study under Professor Hyung Jin Sung's supervision at KAIST in Korea. He also visited Professor Cam Tropea's laboratory at TU Darmstadt in Germany for one year after his graduation. His research interests are the liquid flow rate metrology, the ultrasound flow tomography and the fluid acceleration using LDA.

Byung-Ro Yoon is a principal research technician working at KRISS in Korea. He is working in the field of liquid flow rate and liquid viscosity metrology for more than twenty years. He has an expertise in calibrating and testing various flow meters and viscometers such as the clamp-on type ultrasonic flow meters and the Cannon-Fenske type capillary viscometers, etc.

Kwang-Bock Lee is currently working at Hitrol Co. Ltd. in Korea as a research advisor. He was formerly working at KRISS in Korea as a senior research scientist. He has many experiences in designing and assessing liquid flow rate standard systems. He also has an expertise in consulting with the liquid flow rate standards. His research interests are the liquid flow rate metrology and the development of V-cone flow meters in multi-phase flows.